AIAA SciTech Forum
11–15 & 19–21 January 2021, VIRTUAL EVENT
AIAA Scitech 2021 Forum

10.2514/6.2021-1455

Check for updates

Turbulent Boundary Layer Response to Active Control Plasma Actuator

Mitchell Lozier[1], Flint O. Thomas[2], Stanislav Gordeyev[3]
University of Notre Dame, Notre Dame, IN, 46556

It has been established that the dynamics of large-scale structures (LSS) in the outer region of turbulent boundary layers (TBL) and the near-wall small-scale turbulence are correlated. In the study reported on here, a plasma-based active flow control device was placed within the TBL in order to introduce periodic motions into the wake region. The boundary layer Reynolds number was low enough, $Re_\tau = 700$ that no naturally occurring coherent large-scale structure was present. Via actuation, a periodic synthetic large-scale structure was introduced into the TBL, and the TBL's response to this structure in the near-wall region was studied using a single hot-wire. In previous experiments, it was shown that this large-scale structure had a strong modulating effect on the near-wall turbulence downstream of the actuator. In this study the wake produced by the actuator plate was further characterized and the effect of the synthetic motions on the local skin friction was also analysed. The wake was found to be canonical and a dominant flow feature in the region of the plate, while it was shown that the addition of the plasma forcing lowered the local skin friction when compared to the plate by itself. The TBL response was also measured using a range of actuation frequencies and varied wall-normal actuator positions in order to characterize the significance of the actuation frequency and wall-normal position on the turbulence modulating effect of the LSS. Results show the strongest modulation when the actuation frequency is close to the burst/sweep frequency of the near-wall TBL structure.

I. Introduction

The large-scale structures (LSS) in the turbulent boundary layer (TBL) and their effect on technologically relevant flow properties such as friction drag, noise, aero-optical distortions, and flow separation have been investigated extensively [1] [2] [3] [4]. LSS refers in general to coherent and energetic motions on the order of the boundary layer thickness that dominate the log-linear and wake regions of the TBL in high Reynolds number flows. In the investigations of these LSS, it has been demonstrated that the dynamics of the large-scale motions and the near-wall small-scale turbulence are correlated [3] [5]. Furthermore it was shown that the large-scale motions do not just superimpose a mean velocity change on the near-wall region, they actively modulate the amplitude and organization of the near-wall turbulence. The extent of this interaction increases with the Reynolds number as the energy of the large-scale motions in the outer region becomes comparable to the energy of the coherent near-wall structures. The amplitude modulation that is

[1] Graduate student, Department of Aerospace and Mech. Eng AIAA Student member.
[2] Professor, Department of Aerospace and Mech. Eng., AIAA Associate Fellow
[3] Associate Professor, Department of Aerospace and Mech. Eng., AIAA Associate Fellow

Downloaded by UNIVERSITY OF NOTRE DAME on January 5, 2021 | http://arc.aiaa.org | DOI: 10.2514/6.2021-1455

Copyright © 2021 by Lozier, Thomas and Gordeyev. Published by the American Institute of Aeronautics and Astronautics, Inc., with permission.

imposed on the small scales by these large-scale events importantly demonstrates that the near-wall cycle is not completely autonomous, but rather it is under the influence of the large-scale structures through some outer-inner layer interaction at high enough Reynolds numbers [6]. Similarly the large-scale motions play a role in the redistribution and organization of small turbulent motions throughout the entire boundary layer thickness, not just in the inner region, and a preferential arrangement of small scales relative to the large scales prevails throughout the log-region and wake region [3] [7].

In canonical boundary layers, thin shear layers, separating low-speed and high-speed regions (so-called uniform momentum regions), have been observed and studied in the last few years [5] [6]. These thin shear layer structures, combined with the low momentum flow underneath them, are believed to be parts of a coherent structure, also known as the Attached Eddy. A more recent investigation of adverse pressure gradient TBLs demonstrated that the local flow physics is largely dominated by an embedded shear layer associated with the inflectional instability of the outer mean velocity profile inflection point [7]. Using scaling laws developed for free shear-layers but applied to the adverse pressure gradient (APG) TBL, profiles of mean velocity and turbulence quantities exhibited a remarkable collapse. The generic applicability of the embedded shear layer scaling was demonstrated by collapsing multiple APG turbulent boundary layer data sets from the AFOSR-IFP-Stanford Conference compiled by Coles and Hirst [8]. Further support for the influence of the shear layer structure on the near-wall TBL dynamics was recently provided by a study demonstrating that the presence of a free shear layer just outside a TBL has a significant effect on the near-wall bursting/sweep events [9].

Collectively, the results described above strongly suggest that embedded shear layers are a generic feature of all TBLs irrespective of whether or not the mean velocity profile is inflectional. Although more apparent in APG boundary layers with inherent inflectional mean velocity profiles, transient and non-localized inflectional instabilities could well account for the enhancement of outer large-scale boundary layer structure that has been documented in previous studies of high Reynolds number zero pressure gradient TBLs. These shear-layer-like structures likely play an important role in determining LSS dynamics and ultimately the global properties of the TBL.

An intriguing aspect of the presence of shear layers in the TBL is that they are very amenable to control. The ability to independently control outer layer LSS in the TBL offers new possibilities for uncovering their underlying dynamics. This aspect has been largely unexplored and most studies and models regarding the relationship between the small- and the large-scale structures deal with natural un-manipulated TBLs and apply various conditional-averaging techniques to study their interactions [4]. Only a small number of studies so far have investigated modifying the LSS directly. In [10] an oscillating vertical plate was used to introduce a controlled traveling wave into the log-region of the boundary layer, and triadic interactions between the induced periodic structure and various scales in the boundary layer were studied. In [9] the turbulent boundary layer was externally forced by a shear layer and the turbulence inside the boundary layer was found to be both amplified and modulated by the external forcing.

Inspired by the results in [9], in the current study, active flow control is used to introduce periodic motions into the wake region of the turbulent boundary layer using a plasma based actuator. The boundary layer Reynolds number is low enough, so there are no natural coherent large-scale structures present. By introducing periodic forcing, a synthetic large-scale structure

Downloaded by UNIVERSITY OF NOTRE DAME on January 5, 2021 | http://arc.aiaa.org | DOI: 10.2514/6.2021-1455

was introduced into the outer region of the boundary layer. In [11] it was demonstrated that this periodic active flow control device had sufficient authority within the boundary layer to produce a synthetic large-scale structure with a measurable modulation effect on the near wall small-scale structures.

In this paper, we will further explore the structure of the wake created by the actuator plate and the imposed plasma forcing. This will be useful in understanding the effect of the plate on boundary layer dynamics as well as defining a functional representation of the wake profile that can be superimposed with the canonical boundary layer for modelling purposes. We will also examine how the interaction between the synthetic large-scale structures, introduced by the actuator, and the near-wall turbulence affect the local skin friction. Estimating the changes in skin friction will give a better understanding of the global effect of the synthetic LSS on the boundary layer and will allow analysis of the drag reducing potential of the actuator device. The actuator will then be moved to a wall-normal position closer to the wall in order to determine how the position of the actuator influences the modulation of the near-wall turbulence. Finally we vary the actuation frequency to determine the optimal forcing frequency that will result in the most significant modulation of the near-wall turbulence.

II. Experimental Set-Up

All of the experimental results presented in this paper were obtained using the 2' x 2' subsonic in-draft wind tunnel facility in the Hessert Laboratory at the University of Notre Dame. The overall dimensions of the tunnel test section are 2' x 2' x 7'. For this experiment, a boundary layer development plate 2 meters long with a roughness element attached to the leading edge was installed in the tunnel. A constant temperature anemometer (CTA) with a single boundary layer hot-wire probe (Dantec Type 55P15) with 5 μm diameter and l = 1.5 mm length ($l^+ = 25$) was used to collect time series of the streamwise velocity component. A computer controlled traversing stage was inserted through the top wall of the tunnel along the midpoint of the tunnel span to allow the hot wire anemometer probe to traverse the test section and make measurements at different wall normal or y-locations. The plasma actuator device, as described below, was attached to the top side of the boundary layer development plate at a fixed streamwise location of 140 cm from the leading edge of the boundary layer development plate. The hot wire probe and plasma actuator are shown in Figure 1. The hot wire probe traverse system was also adjustable in the streamwise direction and was positioned at four streamwise or x-locations measured downstream of the plasma actuator trailing edge, in order to measure the TBL response at multiple locations. The locations selected for this experiment were 51 mm, 102 mm, 170 mm, and 272 mm, which correspond to 1.5δ, 3δ, 5δ, and 8δ, respectively, based on the experimentally determined boundary layer thickness. A set of representative turbulent boundary layer characteristics were measured at the downstream location of 3δ using the hot wire probe. These parameters are summarized in Table 1 for reference. The skin friction velocity u_τ was found using the Clauser method. In all of the experiments described below, the tunnel free stream velocity was 7 m/s.

Table 2.1 Turbulent boundary layer parameters at $x = 5\delta$

δ	U_∞	u_τ	C_f	H	Re_θ	Re_τ

Downloaded by UNIVERSITY OF NOTRE DAME on January 5, 2021 | http://arc.aiaa.org | DOI: 10.2514/6.2021-1455

34.8 mm	6.99 m/s	0.298 m/s	0.0037	1.33	1,850	690

A plasma-based Active Large-Scale Structure Actuator (ALSSA) device was used in this experiment to modify the dynamics of the boundary layer. The plasma actuator was supported in the tunnel by two vertical NACA0010 airfoil supports which were 4 mm thick and had a height of H = 21 mm or 0.6δ. The plasma actuator was W = 10 cm wide in the spanwise direction and the plasma actuator length in the streamwise direction was L = 52 mm. The actuator plate was made of a 2 mm thick sheet of Ultem dielectric polymer. The leading edge of the actuator plate was rounded, and the trailing edge was tapered to reduce the separation region behind the trailing edge of the plate. The alternating current (AC) dielectric barrier discharge plasma formed on the actuator was produced using a high voltage AC source which consisted of a function generator, power amplifiers and a transformer [12]. Electrodes on the top and bottom of the actuator were connected to the high voltage AC source which provided a 40kV peak-to-peak sinusoidal waveform excitation to the electrodes at a frequency of 4 kHz. At this high actuation frequency, the plasma operates in a quasi-steady mode, essentially creating a spanwise-uniform steady jet. To introduce periodic forcing, a fifty percent duty cycle was imposed on the waveform, with a repetition frequency, f_p = 50 Hz ($f_P^+ = 0.008$).

A pitot probe was also inserted upstream of the plasma actuator through the side wall of the tunnel to measure the free stream velocity of the tunnel in order to calibrate the hot wire probe. Hot wire voltages, pitot probe pressure transducer voltages and the output of the function generator to the ALSSA device were recorded simultaneously in every test. The data was sampled at f_s = 30 kHz which corresponds to $\Delta t^+ = (1/f_s)u_\tau^2/\nu = 0.2$ for a total period of 150 seconds, or about 25,000 δ/U_∞ in each test. The hot wire probe was conditioned by a low pass filter with a cutoff frequency of 10.4 kHz to eliminate aliasing effects.

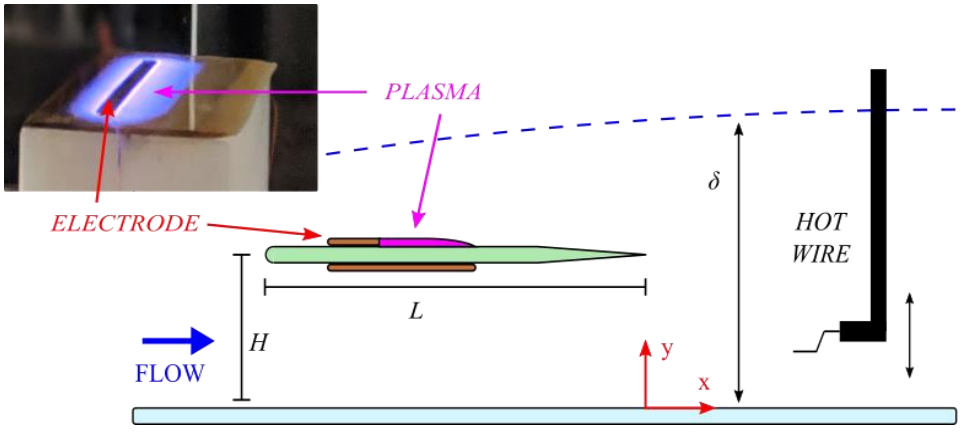

Figure 2.1 Schematic of experimental set-up with picture of plasma-based ALSSA device

III. Results

Downloaded by UNIVERSITY OF NOTRE DAME on January 5, 2021 | http://arc.aiaa.org | DOI: 10.2514/6.2021-1455

The hot-wire anemometer was calibrated before and after each test, using standard methods, and the anemometer voltages were converted into velocities using a linear interpolation between the two calibrations to account for any drift in ambient lab conditions over the course of the experiment. The maximum ambient temperature drift over the course of any experiment was $0.3\ °C$ and the maximum ambient pressure drift over any one experiment was $3\ mbar$. Velocity time series were digitally band-stop filtered in a narrow band around the plasma carrier frequency of $4\ kHz$ to eliminate electronic noise associated with the high voltage AC source supplying the plasma actuator. In the preliminary studies of the ALSSA device, the natural boundary layer was measured at each streamwise measurement location in order to provide a baseline flow and make sure the underlying flow was canonical. Then the plasma actuator was introduced and the boundary layer was measured again with and without the plasma forcing.

For reference,

Figure (a) shows the mean velocity profile of the canonical boundary layer, plasma off and plasma on cases in inner variable scaling for a single measurement location of $x = 5\delta$ with the plate at $y = 0.6\delta$. Near the wall, the mean velocity profiles approach the expected linear scaling of the viscous sublayer although measurements were not taken within the viscous sublayer due to physical restraints of the hot-wire probe traverse system. There is a well-defined log-linear region that extends from approximately $y^+ = 30 - 300$. Using the Clauser method, the log-linear region of the canonical mean profile was fitted to the expected scaling $u^+ = \ln(y^+)/\kappa + \beta$ where $\kappa = 0.385$ and $\beta = 4.1$ in order to determine the local skin friction coefficient and friction velocity as reported in **Error! Reference source not found.**. The friction velocity calculated using the canonical mean profile was used to normalize all of the subsequent turbulence quantities. It should be noted that in the plasma off and plasma on cases the slope of the log-linear region has been modified. An explanation of this change in slope will be explored in later discussion of the estimated local skin friction. At the actuator location of $y^+ = 400$, marked by the vertical dashed line, there is a clear mean velocity deficit due to the wake behind the actuator plate. This velocity deficit is similar in the plasma on case but shifted towards the wall due to the addition of the plasma jet on the top side of the plate.

Figure (b) shows the profile of the root-mean-square of the fluctuating streamwise component of velocity that has been properly normalized by the friction velocity to represent the turbulence intensity in each case. The location of the peak turbulence intensity in each case is located at approximately $y^+ = 15$ which is the expected location for a canonical turbulent boundary layer. The magnitude of the peak turbulence intensity is less than the expected value for a canonical turbulent boundary layer of equivalent Re_τ due to the finite length of the hot-wire. The error in peak intensity is approximately 15 percent which is consistent with the expected spatial attenuation of small-scale turbulence for a hot-wire probe of length $l^+ = 25$ [16]. There is a slight increase in the peak turbulence intensity amplitude for the plasma on and off cases, but the difference is within

Downloaded by UNIVERSITY OF NOTRE DAME on January 5, 2021 | http://arc.aiaa.org | DOI: 10.2514/6.2021-1455

the experimental error. At the actuator location, marked by the vertical dashed line, there is a deficit in the turbulence intensity that is again consistent with the expectation of a wake forming behind the actuator plate. The addition of the plasma jet on the top side of the plate shifts the turbulence intensity deficit towards the wall.

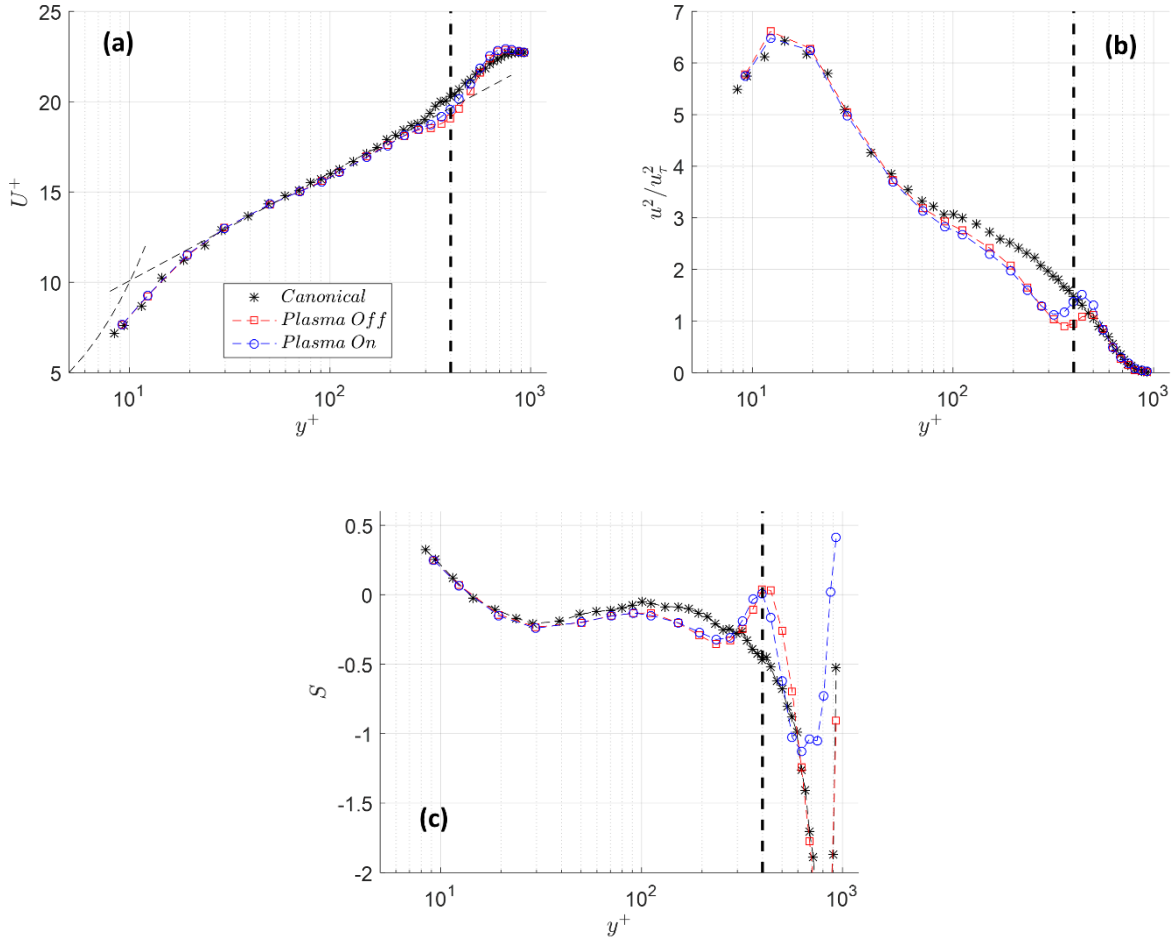

Figure 3.1 TBL profiles of (a) mean velocity (b) turbulence intensity (c) skewness at $x = 5\delta$ with the actuator at $y = 0.6\delta$ and $f_P = 50\ Hz$.

Figure (c) presents the profile of the skewness, defined as the third moment of the fluctuating streamwise component of velocity normalized by the standard deviation, for each case. In the outer region of the boundary layer there is a large negative skewness due to intermittent bursts of turbulent flow entering the freestream regime just outside of the boundary layer. In the plasma on case, this region of negative skewness is reduced greatly due to the periodic large scale motions induced by the actuator contributing additional positive skewness in the same intermittent region.

Downloaded by UNIVERSITY OF NOTRE DAME on January 5, 2021 | http://arc.aiaa.org | DOI: 10.2514/6.2021-1455

The rest of the skewness profile is consistent with the canonical form reported by other studies of TBLs [18]. In the plasma off and plasma on cases the skewness goes towards zero around the actuator location, also marked by the dashed line. This is consistent with the skewness of a symmetric wake forming behind the plate. The observations above, along with calculated parameters such as the shape factor and the growth rate of the turbulent boundary layer affirm the assumption that the baseline flow at each streamwise measurement location is a canonical zero-pressure gradient turbulent boundary layer.

The fact that the skewness is almost exactly zero at the location of the actuator in both modified flows, as compared to -0.5 in the canonical case, confirms that the wake is a dominant feature in the modified flow. Not shown here, the flatness of the fluctuating streamwise component of velocity also goes to zero, the expected value for a Gaussian distribution, at the actuator location reinforcing the idea of a strong and Gaussian wake behind the plate. Because measurements of the plasma off profile were taken repeatedly during the course of parametric studies of the plasma actuator design, the repeatability of these measurements can be demonstrated as seen later in

Figure . To further investigate the structure of the wake behind the plate, the mean velocity profile of the wake was isolated by subtracting the canonical mean profile from the mean profile modified by the actuator plate without plasma forcing as shown in

Figure (a).

The half-width of the wake and the maximum velocity deficit in the wake were measured by fitting the experimental data with a Gaussian function. The Gaussian function was shown to be a simple and appropriate representation of the shape of the wake in these experiments. When the wake profiles were normalized by the half-width and velocity deficit, they exhibited an expected collapse and the fit of the Gaussian distribution can be evaluated from

Figure (b). In

Figure (a) the wake half-width is shown to grow proportionally with the square root of the streamwise distance from the plate. The fit of the half-width data, shown as a dotted line, follows $w = 0.214\sqrt{x + 7.0}\ (mm)$. The maximum velocity deficit,

Figure (b), decays proportionally with the inverse of the square root of the streamwise distance from the plate. The fit of the velocity deficit data, shown as a dotted line, follows $\Delta u = 6.29/\sqrt{x + 7.0}$. These results are consistent with the analytical predictions for a canonical turbulent two-dimensional wake behind a body [17].

From the observations of the skewness and flatness around the actuator plate location, and the demonstration of the canonical development of the wake profile downstream, it was concluded that the wake produced by the plate is of canonical form and is not significantly modified by the turbulent boundary layer. Furthermore these observations demonstrate that the wake behind the plate is a dominant feature of the flow when the actuator plate is introduced. Even at the farthest downstream location of $x = 8\delta$measured in this experiment, there are no measurable influences of TBL structures on the plate wake.

Downloaded by UNIVERSITY OF NOTRE DAME on January 5, 2021 | http://arc.aiaa.org | DOI: 10.2514/6.2021-1455

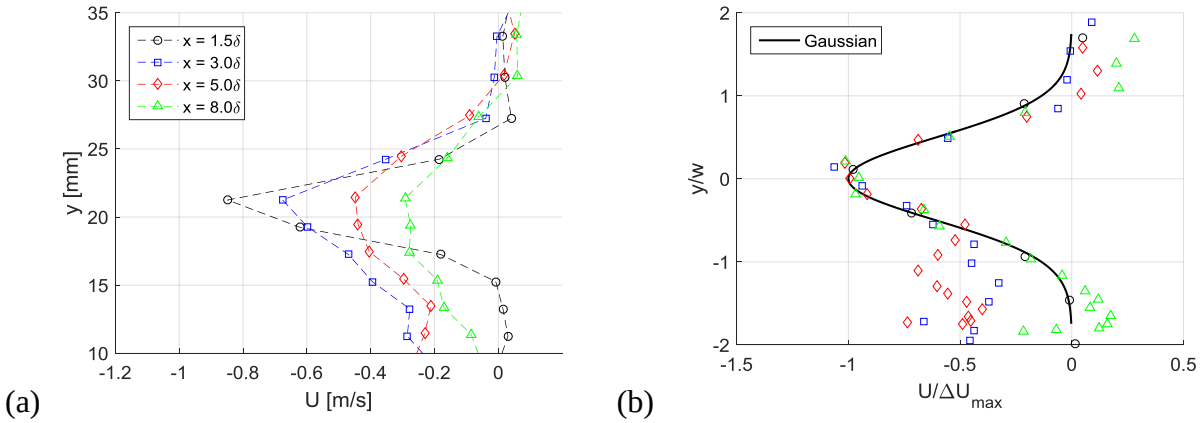

Figure 3.2 Profiles of mean velocity deficit, with no plasma, at each streamwise location in (a) physical units (b) normalized units.

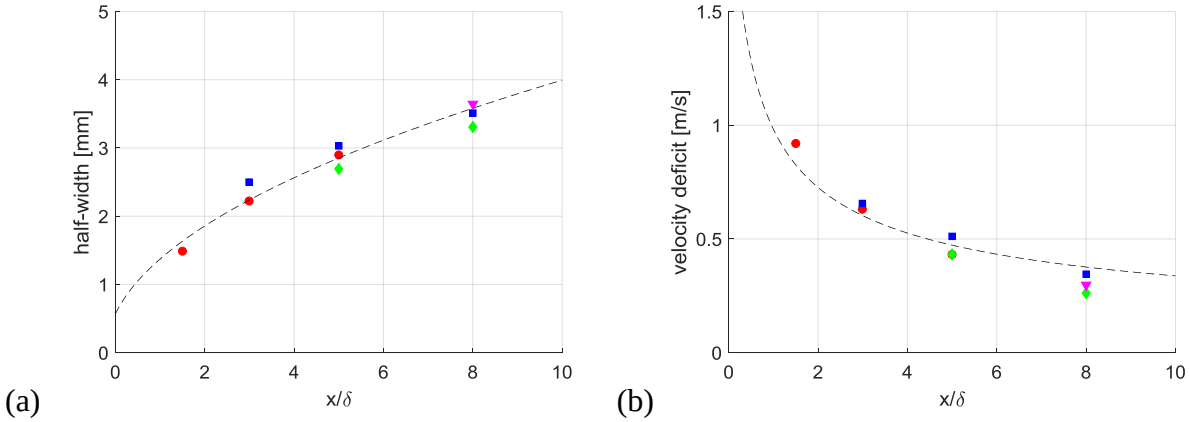

Figure 3.3 Functions of (a) wake half-width (b) mean velocity deficit. Symbols represent different no plasma data sets.

In addition to investigating the wake produced by the plate, the spanwise uniformity of the flow behind the ALSSA device was studied, including the synthetic large scale motions produced by the plasma forcing. A special mount was made for the ALSSA device so that it could be traversed along the tunnel span while the hot-wire was fixed at the center of the tunnel. Measurements were taken in $\Delta z = 6\ mm$ spanwise steps moving 90 mm away from the center of the ALSSA device, which placed the ho-wire outside the airfoil supports. It was assumed that statistically the canonical turbulent boundary layer would be spanwise uniform, but the addition of a plate with finite length along with the airfoil supports at either end of the actuator would result in another smaller region of spanwise uniformity within the bounds of the actuator plate itself. It was also assumed that any non-two-dimensional effects of the ALSSA device would be symmetric about the center of the plate. The streamwise location $x = 8\delta$ was used to evaluate the spanwise

Downloaded by UNIVERSITY OF NOTRE DAME on January 5, 2021 | http://arc.aiaa.org | DOI: 10.2514/6.2021-1455

uniformity because, as shown previously, the wake generated by the plate, and consequently the airfoil supports, will be the widest at the farthest downstream location.

The results of the spanwise studies are presented in Figure 3.4 where the spanwise dependence of the mean and fluctuating velocity components are shown. The location of the airfoil supports are indicated by the black dashed lines, and the center of the actuator plate is at $z = 0$. It was found that there is a region that extends at least $20\ mm$ from the center of the plate in which all of the turbulence quantities are approximately spanwise uniform. This region exists in both the plasma off and plasma on flows as shown by green shading in Figure 3.4.

This spanwise uniformity analysis confirms that the actuator was working as designed, creating two dimensional large-scale motions within the bounds of the actuator plate. This also assures that all previous and subsequent measurements have been made in a region of spanwise uniformity. After confirming the spanwise uniformity of the flow, the hot-wire measurements of mean velocity were used to estimate the local skin friction. The skin friction will demonstrate how effective the synthetic large-scale motions are at modifying the boundary layer dynamics when compared to the plasma off case. The local skin friction can be estimated from the mean velocity profile in a many ways, but not all methods were found to be suitable considering the modified mean flow profiles and experimental limitations.

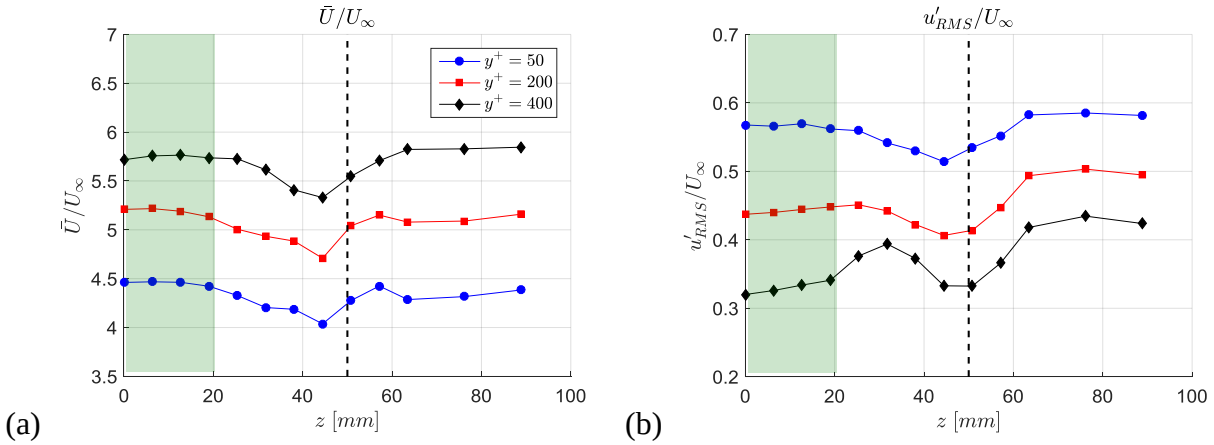

Figure 3.4 Spanwise variation of (a) mean velocity (b) turbulence intensity for selected wall normal locations at $x = 8\delta$ and $y = 0.6\delta\ (y^+ = 400)$. Center of plate is at $z = 0$, airfoil support location indicated by black dashed line.

The changes in mean velocity at the point closest to the wall, approximately $y^+ = 9$ in this case, were measured, and assuming a linear relationship from that point to the wall, the change in slope was used to estimate the wall shear stress. This method is simple but sensitive to errors in the y-position of the hot-wire probe, which are relatively large. This method also relies on measurements being made within the viscous sublayer $y^+ < 5$ which was not always attained, as demonstrated in this particular case. Using another method, the mean velocity profile can be fit to a composite function in the buffer layer [18] or the Clauser function, both of which have the friction velocity as a parameter. The Clauser method, which could be effective due to the changes in slope seen in the log-linear region, has drawbacks when considering the modified velocity profile.

Downloaded by UNIVERSITY OF NOTRE DAME on January 5, 2021 | http://arc.aiaa.org | DOI: 10.2514/6.2021-1455

Specifically, the modification of the mean velocity profile extends from the plate location into the log-linear region reducing the effective region that can be fitted using the Clauser method.

The method chosen for this study uses a fit of the inner and buffer layers, discussed before, through a quadratic function and the composite relationship for the buffer layer, as seen in Equation 3.1. This method was less sensitive to errors in the y-position and still incorporates the velocity profile in the near-wall region which is most sensitive to changes in the local skin friction. The results of estimating the skin friction using this method have been plotted at different streamwise locations in Figure 3.5 in order to show that the addition of the actuator plate decreases the local skin friction coefficient and the addition of plasma actuation provides an additional decrease. The results have been plotted along with measurements done by Savill and Mumford [14] for comparison to relevant parallel plate manipulator experiments. In the results presented here the actuator length was $l = 1.5\delta$, $Re_\theta = 1850$ and the actuator was at a wall-normal height of $y = 0.6\delta$. In the experiments done by Savill and Mumford the actuator length was $l = 1\ or\ 2\delta$, $Re_\theta = 1000$ and the actuator was at a height of $y = 0.5\delta$.

$$y^+ = U^+ + exp(-\kappa B)\left[exp\left(\kappa U^+\right) - 1 - \sum_{n=1}^{3}\frac{(\kappa u^+)^n}{n!}\right] \tag{3.1}$$

Comparing the results, downstream of the actuator plate there is a decrease in the skin friction coefficient, and after it reaches a minimum, it starts to increase again. The current results are consistent with the trend in the comparison data at the measured downstream locations. The results do not match exactly due to the differences in the plate geometry and experimental conditions. The current study also did not measure far enough downstream to compare the locations of maximum skin friction reduction. This analysis shows that in a mean sense the addition of plasma forcing reduces the skin friction, compared to plasma off case. It is important to additionally consider that the skin friction can change throughout the actuation cycle. In order to investigate these potential periodic changes in skin friction, modal analysis was performed to measure the periodic changes in the velocity near the wall.

Downloaded by UNIVERSITY OF NOTRE DAME on January 5, 2021 | http://arc.aiaa.org | DOI: 10.2514/6.2021-1455

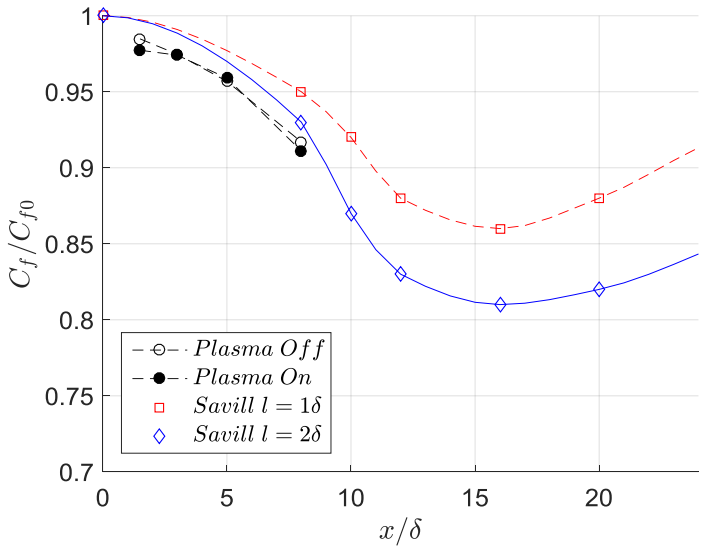

Figure 3.5 Streamwise variation of skin friction $y = 0.6\delta$ and $f_P = 50\ Hz$.

Since the actuator introduced periodic forcing into the flow, it is useful to phase-lock the results to the actuation period following the method utilized in [11]. To do so, a triple phase-locked Reynolds decomposition of the velocity was considered, as shown in Equation 3.2, where u is the instantaneous velocity, U is the time mean component of velocity, $\tilde{u}$ is a phase dependent or modal velocity component, u' is a residual fluctuating turbulent component, φ is the phase, defined by Equation 3.3, where n is a number of realizations.

$$u(y,t) = U(y) + \tilde{u}(y,\varphi) + u'(y,\varphi,n) \tag{3.2}$$

$$\varphi = \left(\frac{t_n}{T_p} - n\right) 2\pi \tag{3.3}$$

The n realizations are single repetition period ($T_p = 1/f_p$) length velocity time series extracted from the overall time series that each begin when the plasma is turned on in the actuation cycle. In Equation 3.3, t_n is a time within the n^{th} realization which is related to the phase angle, φ, by the period of the actuation cycle T_p. The signal produced by the function generator was used to ensure that the data was properly phase locked with the actuation cycle of the plasma. These n realizations of velocity time series are then ensemble averaged to find the modal component of velocity as a function of the phase angle. The fluctuating component of the velocity u' that remains after removing the modal component of velocity from each realization was used to quantify an ensemble-averaged RMS of the residual fluctuations as seen in Equation 3.4.

$$u'_{rms}(y,\varphi) = (\langle [u'(y,\varphi,n)]^2 \rangle_n)^{\frac{1}{2}} \tag{3.4}$$

Downloaded by UNIVERSITY OF NOTRE DAME on January 5, 2021 | http://arc.aiaa.org | DOI: 10.2514/6.2021-1455

Here the square brackets denote ensemble averaging over all realizations. Later we will refer to this quantity as a residual turbulence level. The phase-averaged mean can be removed from the residual turbulence level to define a local change in residual turbulence which will be another quantity of interest. Figure 3.6 shows an example of phase maps of both the modal velocity and residual turbulence at the streamwise measurement location of $x = 5\delta$. In Figure 3.6(a), at the actuator location, indicated by a black dashed line, there is a strong and periodic modal velocity contribution that is concentrated just above the plate. More notably there is a non-zero modal velocity contribution that extends all the way towards the wall and upwards towards the edge of the boundary layer. The periodic changes in modal velocity near the wall will lead to periodic changes in the skin friction as shown in Figure 3.6(c). Although the mean difference in friction coefficient between the plasma on and off cases is small, at various points in the actuation cycle the skin friction is significantly reduced as a result of the plasma forcing.

In the residual turbulence map, shown in Figure 3.6(b), there is a region of strong positive changes in the residual turbulence located around the actuator plate location that has been shown to be related to the synthetic large-scale motions induced by the plasma forcing. There is another region of positive change in residual turbulence near the wall, directly below the region of positive changes around the actuator which will be referred to as the region of modulated near-wall turbulence. The canonical inclination of near-wall structures in higher Reynolds number flows is shown by a red dotted line in Figure 3.6(b). In this case the region of modulated turbulence is more inclined with respect to the wall than the canonical structures. This region of modulated turbulence near the wall is significant because the amplitude modulation is due to the presence of the synthetic large-scale motions and will be vital in studying the dynamics of the TBL.

Downloaded by UNIVERSITY OF NOTRE DAME on January 5, 2021 | http://arc.aiaa.org | DOI: 10.2514/6.2021-1455

Downloaded by UNIVERSITY OF NOTRE DAME on January 5, 2021 | http://arc.aiaa.org | DOI: 10.2514/6.2021-1455

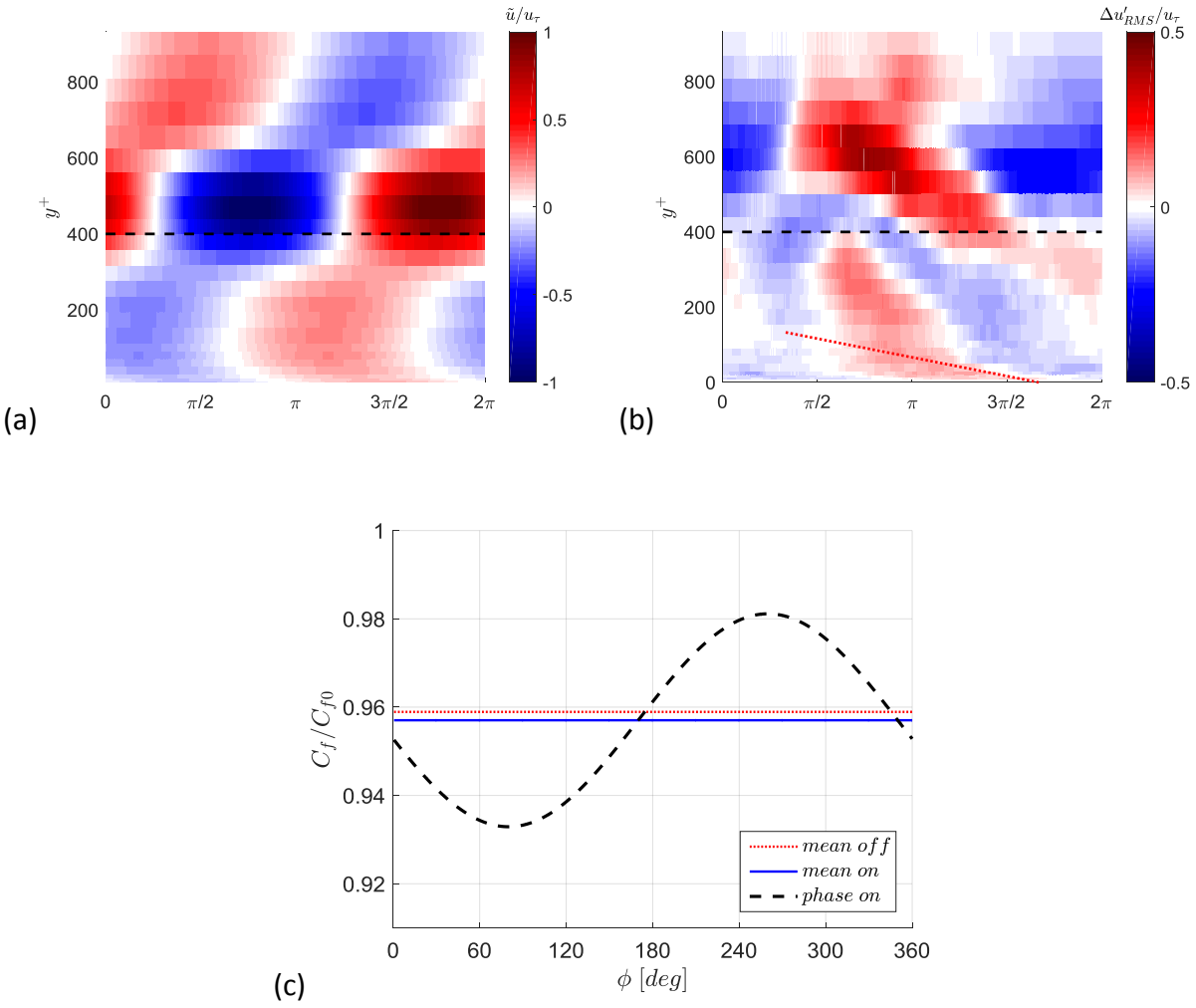

Figure 3.6 Phase maps of (a) modal velocity (b) residual turbulence (c) skin friction at $x = 5\delta$ and $y^+ = 400$ for $f_P = 50\ Hz$. The actuator location is marked by the black dashed line in (a) and (b). Canonical structure inclination is marked by the red dotted line in (b).

In this study, the modal velocity and residual turbulence are used to estimate the strength of the interaction between the synthetic large-scale motions and the near-wall turbulence using a modulation coefficient. The so called Φ-coefficient which was introduced in [11] was used to quantify the modulating effect of the large-scale motions on small-scale motions as shown in Equation 3.5. This modulation coefficient correlates changes in the modal velocity, which represents the large-scale motions, to those in the residual turbulence, which represent small-scale turbulent motions.

$$\phi(y) = \frac{\langle \tilde{u}(y,\varphi)\Delta u'_{rms}(y,\varphi)\rangle_\varphi}{\sqrt{\langle \tilde{u}(y,\varphi)^2\rangle_\varphi}\sqrt{\langle \Delta u'_{rms}(y,\varphi)^2\rangle_\varphi}} \tag{3.5}$$

Figure 3.7 shows the profile of the Φ modulation coefficient for actuator locations of $y^+ = 400$ and $y^+ = 200$. In Figure 3.7 (a), at the actuator y-location, marked by the dotted line, there is a large positive correlation directly below the plate and a negative correlation above the plate. This distinct feature is due to the meandering nature of the wake behind the plate. The regions of positive and negative changes in turbulence intensity downstream of the plate fluctuate due to the periodic plasma forcing being applied only to the top side of the plate. The result of this imbalanced plasma forcing cycle is a wall normal meandering pattern which causes the distinct profile of Φ in that region. There is also a region of strong positive modulation near the wall. This region is an indication that the near-wall turbulent structures are in fact being modulated or reorganized by the synthetic large-scale motions.

Downloaded by UNIVERSITY OF NOTRE DAME on January 5, 2021 | http://arc.aiaa.org | DOI: 10.2514/6.2021-1455

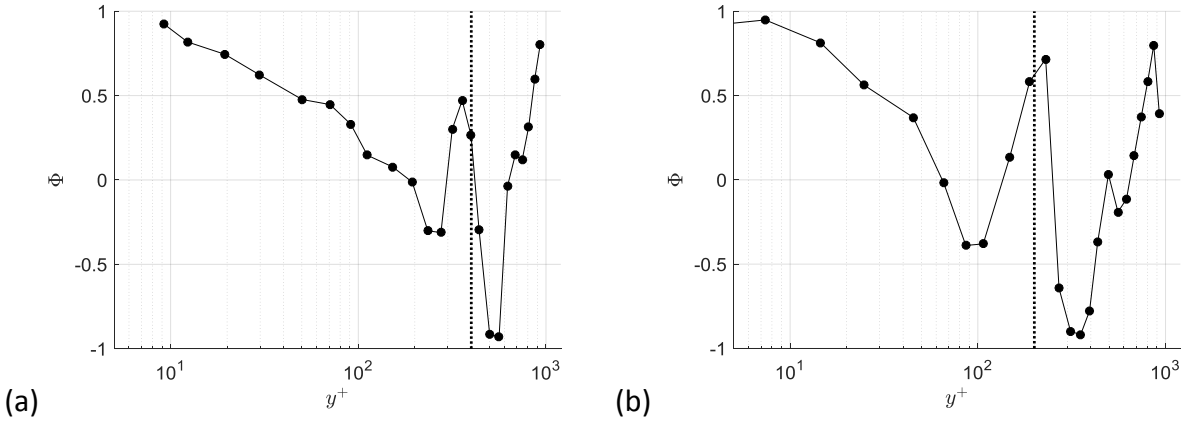

Figure 3.7 Profile of Φ modulation coefficient at $x = 5\delta$ and $f_P = 50\ Hz$ for the actuator y-location of (a) $y = 0.6\delta$ and (b) $y = 0.3\delta$. The actuator location is indicated by the vertical dotted line.

In studies of flat plate manipulators, it was shown that the wall-normal position of the plate affected the performance, specifically the drag reducing capability, of the plate. In order to quantify how the wall normal position of the synthetic LSS changes turbulence quantities and the modulation effect, the actuator was placed to a wall normal location of $y = 0.3\delta$ ($y^+ = 200$) and the actuation frequency was maintained at $50\ Hz$. The analysis techniques used for the wall normal position of $y = 0.6\delta$ were repeated and some of the significant results are presented in Figure 3.8 and Figure 3.9.

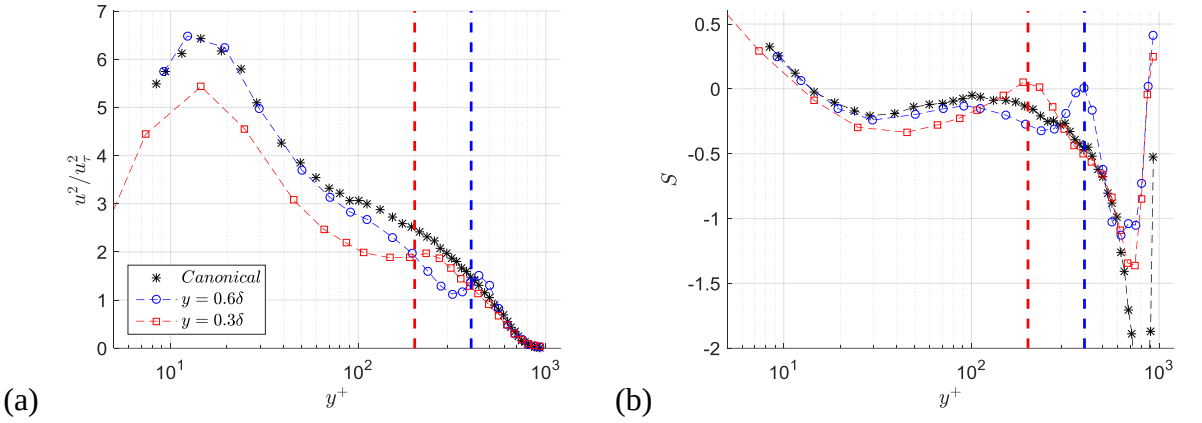

Figure 3.8 Comparison of (a) Turbulence Intensity (b) Skewness at $x = 5\delta$ for $f_P = 50\ Hz$ for different y-location. The actuator locations are indicated by vertical dashed lines.

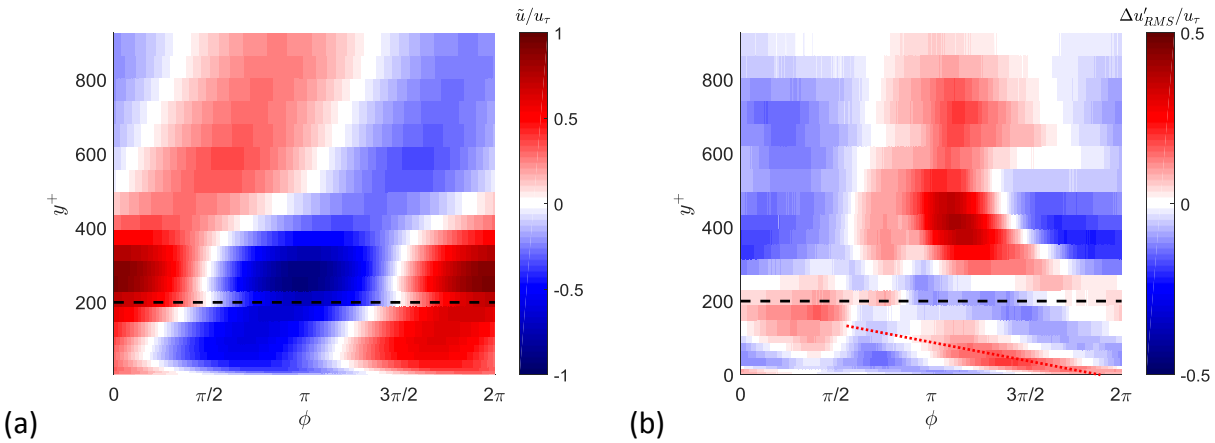

Figure 3.9 Phase maps of (a) modal velocity (b) residual turbulence at $x = 5\delta$ and $y^+ = 200$ for $f_P = 50\ Hz$. The actuator location is marked by the black dashed line. Canonical structure inclination is marked by the red dotted line.

In Figure 3.8(a) in the near-wall region there is a 20% decrease in the turbulence intensity, specifically around the peak. There is also an increase in the negative skewness through the same region in Figure 3.8(b). Not shown here, there is a consistent decrease in the estimated local skin friction when the actuator is moved closer to the wall, and the additional decrease when the plasma forcing is active is larger than the original case where the actuator is farther from the wall. Interestingly, although there are significant changes to the phase maps of modal velocity and residual turbulence seen in Figure 3.9, the strength of the modulation effect is nearly the same as shown in Figure 3.7(b). It appears that moving the actuator closer to the wall creates a stronger direct interaction with structures near the wall, but the modulating and reorganizing effect is left

Downloaded by UNIVERSITY OF NOTRE DAME on January 5, 2021 | http://arc.aiaa.org | DOI: 10.2514/6.2021-1455

unchanged. This leads to the hypothesis that the actuation frequency may be more important in determining the reorganizing effect, which will be studied next.

The frequency of $f = 50\,Hz$ used for the plasma forcing cycle was originally chosen to match the size of naturally occurring large-scale structures of approximately $\lambda = 4\delta$ [4] in higher Reynolds number canonical boundary layers. It was suspected that because this frequency was selected based on outer variable scaling there may exist other plasma forcing frequencies that would lead to a preferred response in the turbulent structures closer to the wall. In order to test this hypothesis the hot-wire probe was placed in the near wall region at $y^+ = 20$ and the frequency of the plasma forcing was varied from 20 to 200 Hz while the actuator was located at $y = 0.6\delta$. The modal velocity and residual turbulence were measured, and the modulation coefficient Φ was computed for each frequency. In Figure 10 the frequency dependent results for Φ are presented. There is a clear band of frequencies around 80 Hz with the largest correlation between large and small scales near the wall.

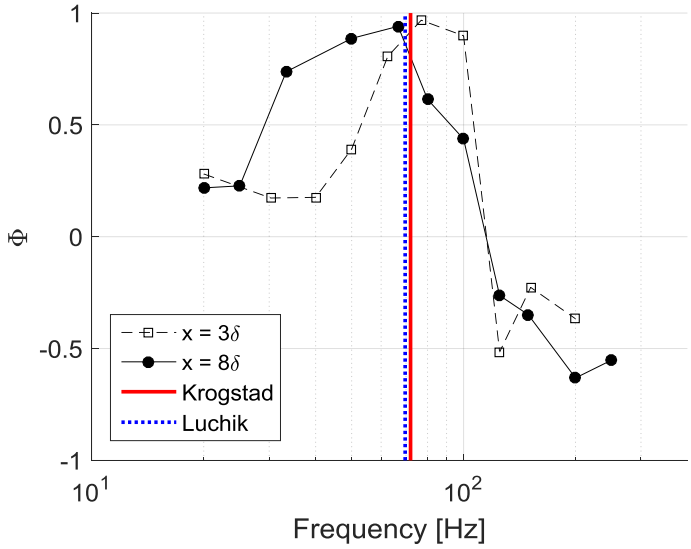

Figure 3.10 Variation of Φ measured at $x = 3\delta$ and $x = 8\delta$ versus the actuation frequency for the actuator located at $y = 0.6\delta$.

Figure 3.10 also shows a few estimations of the bursting frequency [19] from the near-wall cycle which have been overlaid on the profile of the modulation coefficient. The preferred frequency for maximum modulation is very close to the characteristic bursting frequency near the wall. To confirm that the effect of the synthetic large-scale was changed when the frequency was changed, the actuation frequency was increased to 80 Hz and experiments as described above were conducted again. The results, showed in Figure 3.11(b), demonstrate that there are small changes in the organization of the region of modulated residual turbulence near the wall, compared to the results for 50 Hz presented in Figure 3.6. The inclination of the region of modulated turbulence follows the canonical inclination of 15° more closely than the 50 Hz case and resembles the same

Downloaded by UNIVERSITY OF NOTRE DAME on January 5, 2021 | http://arc.aiaa.org | DOI: 10.2514/6.2021-1455

organization as the region of positive modal velocity in the same phase. These changes in organization lead to a much stronger modulation effect at the wall and upwards through the log region as demonstrated in Figure 3.12.

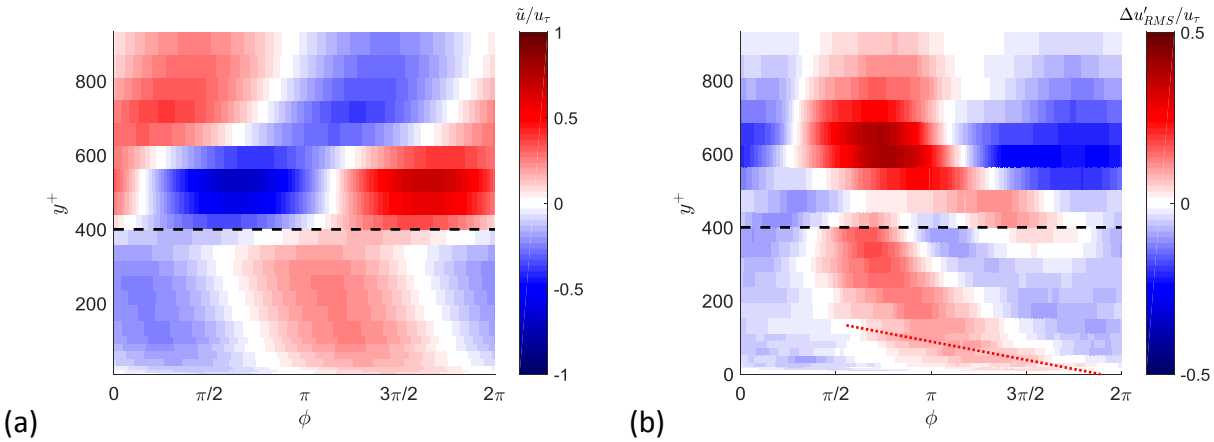

Figure 3.11 Phase maps of (a) modal velocity (b) residual turbulence at $x = 5\delta$ and $y^+ = 400$ for $f_P = 80\ Hz$. The actuation location is marked by the black dashed line. Canonical structure inclination is marked by the red dotted line.

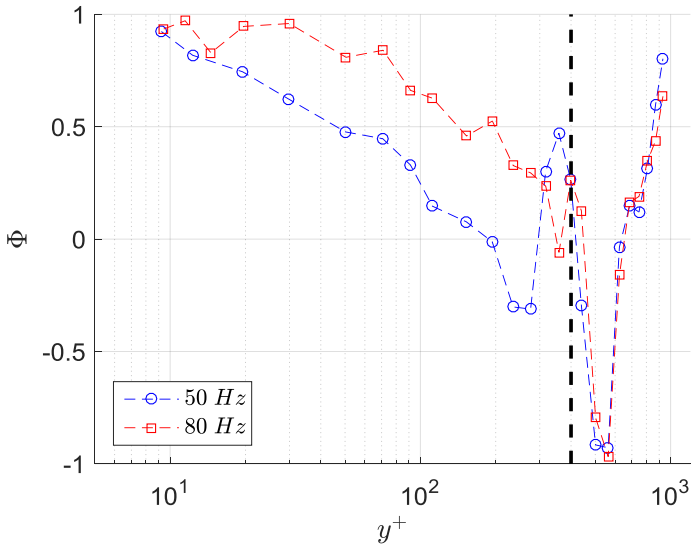

Figure 3.12 Comparison of Φ at $x = 5\delta$ and $y/\delta = 0.6$ for actuation frequencies of $f_P = 50\ Hz$ and $f_P = 80\ Hz$.

Downloaded by UNIVERSITY OF NOTRE DAME on January 5, 2021 | http://arc.aiaa.org | DOI: 10.2514/6.2021-1455

IV. Conclusions

In the study reported here, a plasma-based active flow control device (ALSSA) was placed within the TBL in order to introduce periodic motions into the wake region. The boundary layer Reynolds number was low enough ($Re_\tau = 700$) that no naturally occurring coherent large-scale structures were present in this region. Repeated measurements of the mean velocity downstream of the plate without active plasma forcing were used to investigate the development of the wake created by the plate. The wake was shown to be of the expected canonical form and was more importantly demonstrated so be a dominant feature of the flow in the region downstream of the actuator plate. There were no observed changes to the wake development due to boundary layer structures within the measurement regions. Via plasma forcing, a periodic synthetic large-scale structure was then introduced into the TBL, and the TBL response to this structure in the near-wall region was studied using a single hot-wire. It was demonstrated that centered on the mid span of the plate there is a region where the synthetic motions are two dimensional and the flow downstream of the actuator is spanwise uniform. From the mean velocity the local skin friction was measured and shown to be decreased by the presence of the actuator plate and additionally reduced when the plasma forcing was activated. By performing phase locked analysis, periodic changes in skin friction were estimated showing a total fluctuation of 10% in the skin friction through the actuation cycle. This indicates that at certain phases within the actuation cycle, the addition of the plasma forcing has a significant impact on reducing the skin friction. The phase locked analysis was also used to measure the modulating effect of the synthetic large-scale motions on the near-wall turbulence. When the actuator was moved closer to the wall, the peak turbulence intensity was reduced and the estimated local skin friction was also reduced. However, this change in position did not have a strong effect on the modulation or organization of the near-wall turbulence. By placing the hot-wire probe near the wall, the effect of the plasma forcing frequency was investigated through the modulation coefficient Φ. The frequency results showed that there was a clear band of frequencies closely related to the burst and sweep events of the natural near-wall cycle. When the plasma forcing frequency was increased to maximize the near wall response, there was a change in the organization of the near-wall turbulence as well as a strong increase in the modulating effect of the LSS from the wall through the log region.

V. Acknowledgments

This work is supported by Office of Naval Research, Grant number N00014-18-1-2534. The U.S. Government is authorized to reproduce and distribute reprints for governmental purposes notwithstanding any copyright notation thereon.

Downloaded by UNIVERSITY OF NOTRE DAME on January 5, 2021 | http://arc.aiaa.org | DOI: 10.2514/6.2021-1455

VI. References

[1] M. Guala, S. E. Hommema and R. J. Adrian, "Large-scale and very large-scale motions in turbulent pipe flow," *J. Fluid Mech.,* vol. 554, pp. 521-542, 2006.

[2] R. Mathis, N. Hutchins and I. Marusic, "Large-Scale Amplitude Modulation of the Small-Scale Sturcutres in Turbulent Boundary Layers," *J. Fluid Mech.,* vol. 658, pp. 311-336, 2009.

[3] N. Hutchins and I. Marusic, "Large-scale influences in near-wall turbulence," *Phil. Trans. R. Soc. A,* vol. 365, pp. 647-664, 2007.

[4] S. K. Robinson, "Coherent Motions in the Turbulent Boundary Layer," *Ann. Rev. Fluid Mech.,* vol. 23, pp. 601-639, 1991.

[5] R. Mathis, N. Hutchins and I. Marusic, "A predictive inner-outer modle for streamwise turbulence statistics in wall-bounded flows," *J. Fluid Mech,* vol. 681, pp. 537-566, 2011.

[6] R. J. Adrian, C. D. Meinhart and C. D. Tomkins, "Vortex organization in the outer region of the turbulent boundary layer," *J. Fluid Mech.,* vol. 422, pp. 1-53, 2000.

[7] C. M. de Silva, N. Hutchins and I. Marusic, "Uniform momentum zones in turbulent boundary layers," *J. Fluid Mech.,* vol. 786, pp. 309-331, 2016.

[8] I. Marusic and J. P. Monty, "Attached Eddy Model of Wall Turbulence," *Ann. Rev. Fluid Mech.,* vol. 51, pp. 49-74, 2019.

[9] D. M. Schatzman and F. O. Thomas, "An experimental investigation of an unstready adverse pressure gradient turbulent boundary layer: embedded shear layer scaling," *J. Fluid Mech.,* vol. 815, pp. 592-642, 2017.

[10] D. E. Coles and E. A. Hirst, "Comutation of Turbulent Boundary Layers: Compiled Data," in *AFOSR-IFP,* Stanford University, 1968.

[11] P. Ranade, S. Duvuuri, B. McKeon, S. Gordeyev, K. Christensen and E. J. Jumper, "Turbulence Amplitude Amplification in an Externally Forced, Subsonic Turbulent Boundary Layer," *AIAA Journal,* vol. 57, pp. 3838-3850, 2019.

[12] T. C. Corke and F. O. Thomas, "Active and Passive Turbulent Boundary-Layer Drag Reduction," *AIAA Journal,* vol. 56, 2018.

[13] T. C. Corke, Y. Guezennec and H. M. Nagib, "Modification in drag of turbulent boundary layers resulting from manipulation of large-scale strucutres," NASA CR-3444, 1981.

[14] A. M. Savill and J. C. Mumford, "Manipulations of turbulent boundary layers by outer-layer devices: skin-friction and flow-visualization results," *J. Fluid Mech.,* vol. 191, pp. 389-418, 1988.

[15] F. O. Thomas, T. C. Corke, M. Iqbal, A. Kozlov, "Optimization of SDBD Plasma Actuators for Active Aerodynamic Flow Control," *AIAA Journal,* vol. 47, pp. 2169-2178, 2009.

[16] N. Huthcins, T. B. Nickels, I. Mausic and M. S. Chong, "Hot-wire spatial resolution issues in wall-bounded turbulence," *J. Fluid Mech.,* vol. 635, pp. 103-136, 2009.

[17] H. Schlicting, Boundary Layer Theory, 9th ed., Springer, 2017.

[18] D. B. Spalding, "A single formula for the law of the wall," *J. Appl. Mech.,* vol. 28, pp. 455-457, 1961.

[19] T. S. Luchik and W. G. Tiederman, "Timescale and structure of ejections and busts in turbulent channel flows," *J. Fluid Mech.,* vol. 174, pp. 529-552, 1987.

Downloaded by UNIVERSITY OF NOTRE DAME on January 5, 2021 | http://arc.aiaa.org | DOI: 10.2514/6.2021-1455